Title
Engineering Catalyst–Electrolyte Microenvironments to Optimize the Activity and Selectivity for the Electrochemical Reduction of CO2 on Cu and Ag

Journal
Accounts of Chemical Research, 55(4)

ISSN
0001-4842

Authors
Bui, Justin C
Kim, Chanyeon
King, Alex J
et al.

Publication Date
2022-02-15

DOI
10.1021/acs.accounts.1c00650

Peer reviewed

Engineering Catalyst-Electrolyte Microenvironments to Optimize the Activity and Selectivity for Electrochemical Reduction of CO_2 on Cu and Ag

Justin C. Bui[†1,2], Chanyeon Kim[†1,2], Alex J. King[1,2], Oyinkansola Romiluyi[1,2], Ahmet Kusoglu[3], Adam Z. Weber[2,3], Alexis T. Bell[1,2]*

[1] Department of Chemical and Biomolecular Engineering
University of California, Berkeley
Berkeley, CA 94720, USA

[2] Liquid Sunlight Alliance
Lawrence Berkeley National Laboratory
Berkeley, CA 94720, USA

[3] Energy Technologies Area
Lawrence Berkeley National Laboratory
Berkeley, CA 94720, USA

Accounts of Chemical Research
October 15, 2021

[†]Contributed equally

***Corresponding Author**
email: alexbell@berkeley.edu
phone: (510) 459-4322

1. Conspectus

The electrochemical reduction of carbon dioxide (CO_2R) driven by renewably generated electricity (e.g., solar and wind) offers a promising means for reusing the CO_2 released during the production of cement, steel, and aluminum, as well as the production of ammonia and methanol. If CO_2 could be removed from the atmosphere at acceptable costs (i.e., < $100/t of CO_2), then CO_2R could be used to produce carbon-containing chemicals and fuels in a fully sustainable manner. Economic considerations dictate that CO_2R current densities must be in the range of 0.1A/cm^2 to 1 A/cm^2 and selectivity toward the targeted product is high in order to minimize separation costs. Industrially relevant operating conditions can be achieved by using gas diffusion electrodes (GDEs) to maximize the transport of species to and from the cathode and combining such electrodes with a solid-electrolyte membrane by eliminating the ohmic losses associated with liquid electrolytes. Additionally, high product selectivity can be attained by careful tuning of the microenvironment near the catalyst surface (e.g., the pH, the concentrations of CO_2 and H_2O, and the identity of the cations in the double layer adjacent to the catalyst surface).

We begin this Account with a discussion of our experimental and theoretical work aimed at optimizing catalyst microenvironments for CO_2R. We first examine the effects of catalyst morphology on the production of multicarbon (C_{2+}) products over Cu-based catalysts and then explore the role of mass transfer combined with the kinetics of buffer reactions on the local concentration of CO_2 and pH at the catalyst surface. This is followed by a discussion of the dependence of local CO_2 concentration and pH on the dynamics of CO_2R and the formation of specific products. Next, we explore the impact of electrolyte cation identity on the rate of CO_2R and the distribution of products. Subsequently, we look at utilizing pulsed electrolysis to tune the local pH and CO_2 concentration at the catalyst surface. The last part of the discussion demonstrates that ionomer-coated catalysts in combination with pulsed electrolysis can enable the attainment of very high (> 90 %) selectivity to C_{2+} products over Cu in aqueous electrolyte. This part of the Account is then extended to consider the difference in catalyst-nanoparticle microenvironment, present in the catalyst layer of a membrane electrode assembly (MEA), to that of a planar electrode immersed in an aqueous electrolyte.

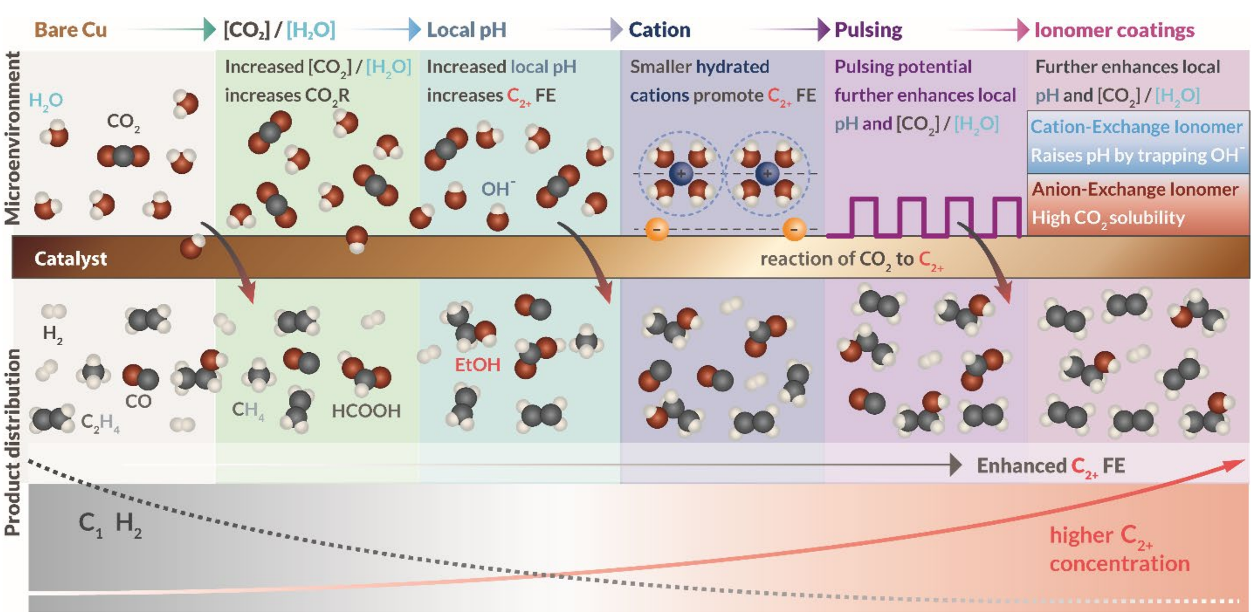

2. Key References

(1) Singh, M. R.; Clark, E. L.; Bell, A. T. Effects of Electrolyte, Catalyst, and Membrane Composition and Operating Conditions on the Performance of Solar-Driven Electrochemical Reduction of Carbon Dioxide. *Phys. Chem. Chem. Phys.* **2015**, *17*, 18924–18936. https://doi.org/10.1039/c5cp03283k.

Explores the impact of mass transport on the electrochemical performance and product selectivity observed in an electrochemical CO_2 reduction device through the means of experiment and macroscale, continuum simulation.[1]

(2) Resasco, J.; Chen, L. D.; Clark, E.; Tsai, C.; Hahn, C.; Jaramillo, T. F.; Chan, K.; Bell, A. T. Promoter Effects of Alkali Metal Cations on the Electrochemical Reduction of Carbon Dioxide. *J. Am. Chem. Soc.* **2017**, *139*, 11277–11287. https://doi.org/10.021/jacs.7b06765.

Demonstrates the impact of the choice of alkali metal cation on the C_{2+} selectivity of electrochemical CO_2 reduction on Cu catalysts, demonstrating that alkali cations with smaller hydrated radii pack more tightly in the outer Helmholtz plane and stabilize intermediate adsorption.[2]

(3) Kim, C.; Weng, L. C.; Bell, A. T. Impact of Pulsed Electrochemical Reduction of CO_2 on the Formation of C_{2+} Products over Cu. *ACS Catal.* **2020**, *10*, 12403–12413. https://doi.org/10.1021/acscatal.0c02915.

Reveals the impacts of pulsed cathodic potential operation on the observed selectivity and performance of CO_2 reduction on Cu catalysts, demonstrating that pulsed operation enables a substantial enhancement in the selectivity towards C_{2+} products due to an increase in the local CO concentration during dynamic operation.[3]

(4) Kim, C.; Bui, J. C.; Luo, X.; Cooper, J. K.; Kusoglu, A.; Weber, A. Z.; Bell, A. T. Tailored Catalyst Microenvironments for CO_2 Electroreduction to Multicarbon Products on Copper Using Bilayer Ionomer Coatings. *Nat. Energy* **2021**, *6*, 1026–1034. https://doi.org/10.1038/s41560-021-00920-8.

Develops bilayer, ion-conducting polymer coatings for Cu catalysts that carefully tune the local CO_2, water content, and pH to optimize selectivity for C_{2+} products, and provides physical and mechanistic insight for the enhancement of C_{2+} selectivity with these ionomer-coated catalyst materials.[4]

3. Introduction

The rise in the atmospheric concentration of CO_2 has stimulated research devoted to its capture and utilization to produce chemicals and fuels, with the energy provided by renewable sources, such as wind and solar irradiation. If direct air capture of the CO_2 can be done at a cost of < \$100/t, then one could envision a closed-loop cycle for producing chemicals and fuels with no net CO_2 emissions.[5] Electrochemical reduction of CO_2 (CO_2R) has emerged as a promising means for converting CO_2 into useful products. Technoeconomic analyses have demonstrated that CO_2R current densities in the range of 0.1 to 1 A/cm^2 and selectivity to multicarbon (C_{2+}) products >80% faradaic Efficiency (FE) are required to make CO_2R economically attractive.[5] Targeted CO_2R current densities and selectivity can be achieved through the use of gas-diffusion electrodes (GDEs) to maximize transport of species and tuning of the chemical microenvironment near the catalyst surface, respectively.[3,4,6–8]

This Account examines how various factors influencing the microenvironment immediately adjacent to the catalyst surface alter catalyst activity and selectivity for CO_2R. In this context, we examine the effects of mass transfer on the local pH and CO_2 concentration near the catalyst surface, and how the choice of electrolyte cation affects the strength of the electrostatic field in the Helmholtz double layer.[2,9,10] We show that further control of the microenvironment can be achieved by deposition of thin ionomer layers over the catalyst and by using pulsed, rather than static, electrolysis.[4] We then turn our attention to the difference in microenvironments in a porous catalyst layer, present in a membrane-electrode assembly (MEA), and planar electrodes immersed in an aqueous electrolyte. Within an MEA, the catalyst nanoparticles in the porous catalyst layer are covered by ionomer, electrolyte, and gases,[6] creating a complex microenvironment that, at the moment, is poorly understood.

4. Effects of microenvironment on the CO_2R on Cu and Ag

Extensive research by Hori and others, has shown that product selectivity is strongly dependent on the metal used as the cathode.[11–14] Sn exhibits high selectivity to formic acid and HCOOH, Ag and Au exhibit high selectivity to CO, and only Cu exhibits high selectivity for the formation of multicarbon hydrocarbons and oxygenated compounds.[14] Prior work has also shown that the structure of the catalyst plays an important role in the product distributions observed on various catalysts.[14–16] In this Account, we focus primarily Cu and Ag catalysts since are can produce C_{2+} products and CO, respectively, with high faradaic efficiency. In the case of Cu, surface roughening to create undercoordinated Cu atoms enhances the formation of C_{2+} products and reduces the formation of H_2 and C_1 products. Since C_{2+} products (e.g., ethylene, ethanol, and propanol) are suitable intermediates for producing a wide variety of chemicals and fuels, substantial efforts have been devoted to identifying methods to alter the microenvironment near the catalyst surface to enhance the C_{2+} product selectivity. In the case of Ag, maximizing the ratio of CO to H_2 can be achieved by increasing the local pH or enhancing the local concentration of CO_2.

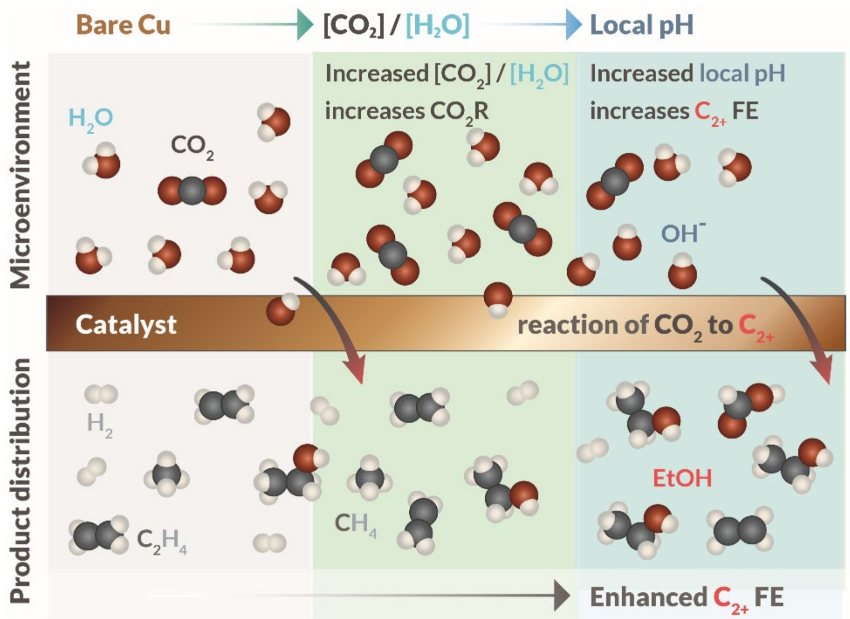

Figure 1: Effects of local microenvironment on CO_2R over a Cu catalyst. Shown are the effects of high local CO_2/H_2O ratio on the rate of CO_2R and the effect of high local pH on the FE to C_{2+} products.

A schematic showing how the microenvironment near the catalyst surface influences the rate at which CO_2R occurs and its product distribution is given in **Figure 1**. A high ratio of the local concentrations of CO_2 to H_2O enhances the rate of CO_2R, whereas a high local pH suppresses the formation of H_2 and C_1 relative to C_{2+} products.[16,17] While not shown in this figure, the microenvironment at the catalyst surface is also influenced by the identity of the electrolyte cations and anions, and by coating the surface with thin films of ionomer.

Lastly, it is critical to note that this introduction to the effects of microenvironment on catalyst performance is done with the aim of giving the reader an understanding of the manner in which the microenvironment can be engineered in order to achieve high activities and selectivities to targeted products of CO_2R. More comprehensive reviews of many of the topics treated in this Account can be found in Refs. 14, and 18-25.[14,18–25]

4.1 Impact of mass-transfer effects

During CO_2R in an aqueous electrolyte, H_2O is consumed by the reduction of CO_2, and OH^- anions are produced, viz., $H_2O + CO_2 + 2\ e^- \rightarrow CO + 2\ OH^-$. The CO_2 consumed at the cathode must be supplied by mass transfer from the bulk electrolyte and the OH^- anion must transport from the cathode surface to the bulk electrolyte. The gradients in CO_2 and OH^- created by these processes are sharpened by the occurrence of bulk reactions involving CO_2 and OH^- anion, which produce HCO_3^- and CO_3^{2-}:

$$\mathrm{CO_2(aq) + H_2O} \quad \leftrightarrow \mathrm{H^+ + HCO_3^-} \tag{1}$$

$$\mathrm{HCO_3^-} \quad \leftrightarrow \mathrm{H^+ + CO_3^=} \tag{2}$$

$$\mathrm{CO_2(aq) + OH^-} \quad \leftrightarrow \mathrm{HCO_3^-} \tag{3}$$

As the cathode current density increases, the local concentration of CO_2 decreases and that of OH^- increases, resulting in a substantial increase in the local pH. Computational and experimental studies have shown that the local concentration of CO_2 at the catalyst surface approaches 0 mM (as opposed to the 34 mM of saturated CO_2 in an aqueous electrolyte) due to consumption of CO_2 by both CO_2R and parasitic electrolyte buffer reactions (equations 1-3). Conversely, the pH can rise as much as 4 pH units as a result of the stoichiometric generation of OH^- anions during CO_2R.[1,8,26,27]

The effects of mass transport on the surface concentrations of species are critical to consider because the kinetics of each product generated by CO_2R are dependent on the local concentration of CO_2, the pH, and the overpotential for that reaction. The kinetics for each product have been measured and the product current density can be expressed by a Tafel relationship,[28]

$$i_k = -i_{o,k}\left(\frac{c_{CO_2}}{c_{ref}}\right)^{\gamma_{CO_2,k}} \exp\left(-\gamma_{pH,k,SHE}\, pH\right) \exp\left(-\frac{\alpha_{c,k}F}{RT}(\eta_k)\right). \tag{4}$$

In Eq. **(4)**, $i_{o,k}$ is the exchange current density for product k, $\gamma_{CO2,k}$ is the CO_2 reaction order, $\gamma_{pH,k}$ is the sensitivity of the current density to pH, and $\alpha_{c,k}$ and η_k are the transfer coefficient and overpotential for product k, respectively.

We note that the Tafel rate equation assumes a single rate-determining step for which all other steps are quasi equilibrated, and it uses semi-empirical lumped parameters to describe the charge transfer in the rate-determining step. Additionally, the effects of the electrical double layer are contained implicitly in the charge-transfer coefficient and exchange current density. Nevertheless, the importance of controlling the local CO_2 and pH becomes clear, since the rate of the CO_2R conversion to each product is directly dependent on these local concentrations. This understanding motivates engineering the chemical microenvironment as a means to achieve high total current densities and the desired product distribution for CO_2R.

4.2 Impact of the electrolyte cation and anion

In aqueous CO_2R, the cations and anions from the electrolytic salt are essential components of the microenvironment near the catalyst surface, where these ions can influence selectivity. We have investigated the effects of alkali metal/bicarbonate (HCO_3^-) electrolytes, Li^+, Na^+, K^+, Rb^+, and Cs^+, on CO_2R in order to understand better their impact on product formation over Cu.[2,9,29] Partial current densities corresponding to the formation of $HCOO^-$, C_2H_4, and C_2H_5OH demonstrated an increase with respect to the atomic radius of the cation, $Li^+ < Na^+ < K^+ < Rb^+ < Cs^+$, while those for H_2, CO, and CH_4 did not change significantly.[2,29] Additionally, when a mixture of $LiHCO_3$ and $MHCO_3$ (M = Na^+, K^+ or Cs^+) was used as the electrolyte, the product distribution more closely resembled that obtained in the presence of $MHCO_3$ even when Li^+ cations were only 10% of the total.[2] Theoretical calculations revealed that the observed effects of cation identity are attributable to the strength of the electrostatic field in the double layer, which increases with decreasing radius of the hydrated cation in the outer Helmholtz plane and increasing PZC of the metal catalyst.[2,29] The increase in the electrostatic field as the hydrated cation decreases stabilizes adsorption of surface intermediates having significant dipole moments (e.g., $*CO_2$, *OCCO), thereby increasing CO_2R activity and C_{2+} selectivity (**Figure 2**).[29]

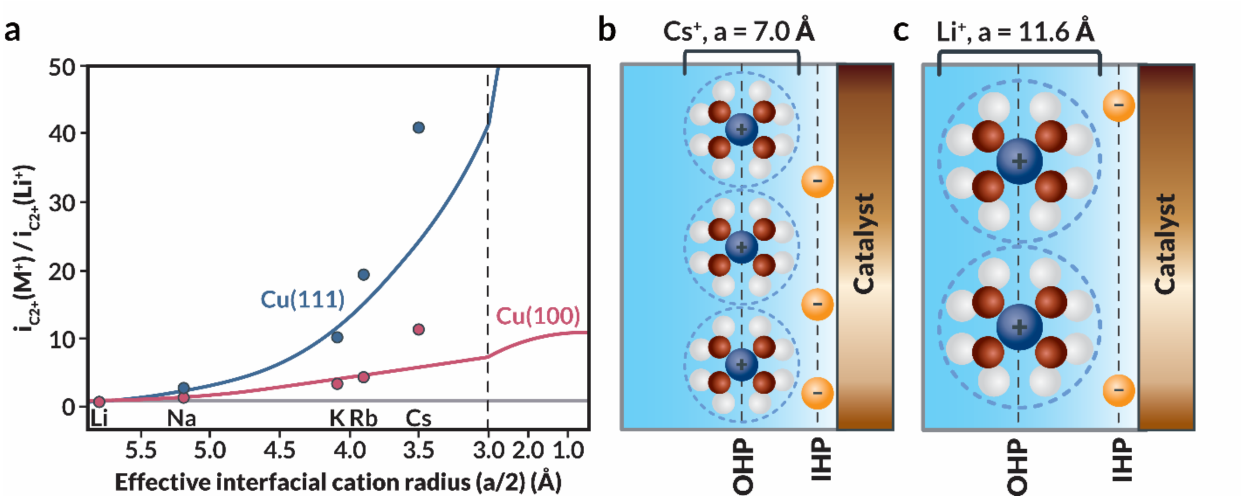

Figure 2: Effect of the electrolyte cation on electrochemical CO_2R on a Cu catalyst.[29] **(a)** C_{2+} current density measured in an $MHCO_3$ electrolyte normalized by that measured in an $LiHCO_3$ electrolyte. The blue line is for Cu(111) and the red line is for Cu(100). Points and lines represent the experimental data and theoretical predictions, respectively. **(b, c)** Illustration of the impact of the size of the hydrated cation on charging of the catalyst surface.

To elucidate the fundamental influence of cations, a multiscale, multiphysics modeling approach is required. Our group has undertaken such an effort for CO_2R on Ag in an aqueous electrolyte. Density functional theory (DFT) was used to predict the rate coefficients needed for the microkinetic model, which was then coupled with a continuum transport model.[10] This approach provided an understanding of the reaction kinetics and surface species present on Ag during CO_2R and revealed that the rate-limiting step for CO_2R on Ag involves hydrogenation of adsorbed CO_2 ($*CO_2^{\delta-}$). The studies showed that hydrated cations with smaller radii present near the surface of Ag stabilize $*CO_2^{\delta-}$ through electrostatic interactions,[10] leading to higher coverages and, subsequently, higher rates of CO formation, in agreement with experimental observation.[29] Although the complex nature of CO_2R on Cu makes similar studies exceedingly difficult, the findings of this multiscale, multiphysics investigation on Ag demonstrate that cations play a critical role in stabilizing partially charged intermediates, thereby impacting CO_2R product distributions.

We have also investigated the impact of anions on CO_2R over Cu. Anions with buffering capacity, such as bicarbonate, borate (H_3BO_3), and phosphate (HPO_4^{2-}), as well as those without buffering capacity, such as perchlorate (ClO_4^-) and sulfate (SO_4^{2-}), were examined at a fixed potassium cation concentration of 0.1 M.[30] While anions without buffering capacity exhibited no noticeable influence, buffering anions demonstrated an increase in selective formation of H_2 and CH_4 in the order $HCO_3^- < H_3BO_3 < HPO_4^{2-}$. This finding was attributed to the decreasing trend in their pK_a—HCO_3^- (10.33) > H_3BO_3 (9.23) > HPO_4^{2-} (7.21), which is consistent with the fact that the rate of H_2 formation is limited by the rate of H atom formation on the catalyst surface via proton-electron transfer, and that the rate of CH_4 formation is limited by the rate of *CO hydrogenation.

4.3 Pulsed CO_2 electrolysis

Controlling the cathode potential dynamically is a facile means for modulating the catalyst microenvironment and, therefore, the CO_2R product distribution. Of particular interest is the performance of CO_2R when the cathodic potential is repeatedly alternated between two distinct potential setpoints (i.e., pulsing). Many prior studies of pulsed-CO_2R focused on the pulse-derived reconstruction of the catalyst surface because the cathode potentials were chosen above and below the standard reduction potential of the catalyst (i.e., +0.42 V vs RHE for Cu), resulting in continuous redox of the catalyst surface.[31–37] However, improved selectivity toward CO_2R over hydrogen evolution compared to static electrolysis is observed even when both potential setpoints were more negative than the standard reduction potential of the catalyst (see **Figure 3)**. This observation implies that pulsed electrolysis can be used to modulate reaction dynamics by perturbating the microenvironment within the vicinity of the catalyst.[3,36–38]

To investigate the pulsing effect, we employed differential electrochemical mass spectroscopy (DEMS) in tandem with gas chromatography and high-pressure liquid chromatography to analyze both local and bulk concentrations of CO_2R products. DEMS measurements collected *in situ* during CO_2R facilitated direct observation of product-evolution hysteresis between cathodic (more negative potential) and anodic (less negative potential) scans (see **Figure 3a**). Specifically, the generation CO and C_2H_4 was increased in the anodic scan compared to the cathodic scan while that of H_2 exhibited contrary behavior. The two cathodic potential setpoints for pulsed electrolysis were set at −0.8 and −1.15 V vs. RHE to maximize the difference in generation rates between the cathodic and anodic scan, with an optimal duration of 10 s. Relative to static electrolysis at the time-averaged potential, the FE of C_{2+} products increased from 60% to 81% while FE of H_2 decreased from 22% to 9%. DEMS data revealed that the distribution of products generated locally during pulsed electrolysis were distinctly different from those observed for static electrolysis, suggesting differences in the chemical microenvironments between the two electrolysis modes.

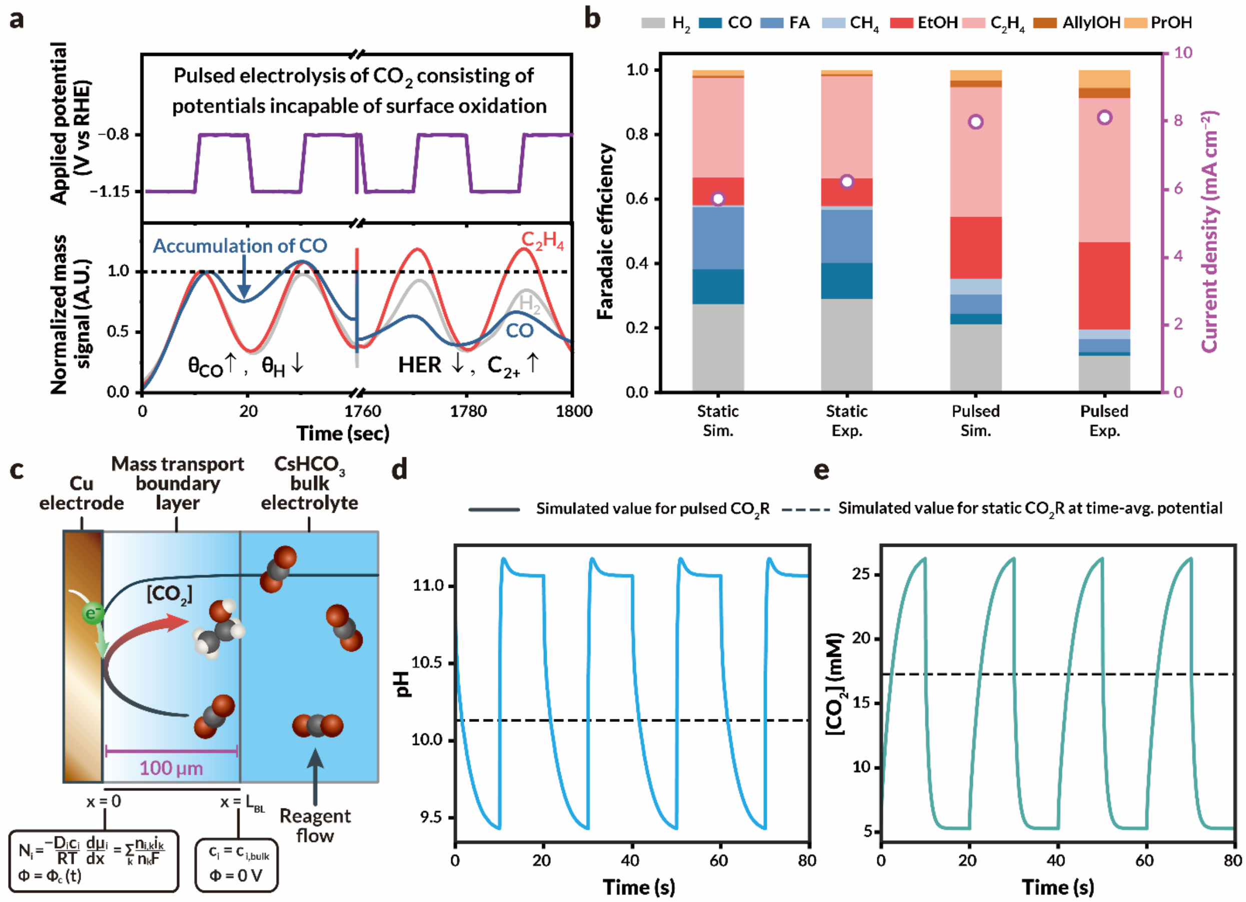

Figure 3: Overview of study of pulsed electrolysis on Cu catalysts.[3,8] **(a) Top panel:** Rectangular wave applied potential signal used in pulsed electrolysis ($\Phi_1 = -1.15$ V vs. RHE, $\Phi_2 = -0.8$ V vs. RHE, and $t_1 = t_2 = 10$ s). **Bottom panel:** Measured DEMS signal of local C_2H_4, H_2, and CO concentrations at the Cu catalyst surface. **(b)** Simulated and experimental product distributions and total current density for static and pulsed electrolysis. Static results represent a product distribution taken for static electrolysis at the time-averaged potential. **(c)** Schematic representation of the simulated domain for the boundary layer model and its boundary conditions. Simulated **(d)** local pH and **(e)** local CO_2 concentration for pulsed (solid lines) and static electrolysis (dashed line).

To explain the difference in microenvironments of pulsed and static electrolysis, we developed a time-dependent, continuum model of the mass-transport boundary layer next to the Cu surface (see **Figure 3c**). The electrode surface reactions were modeled using concentration-dependent Tafel kinetics fit to experimental data of static CO_2R on a planar Cu catalyst.[8] Since the reaction kinetics used in these simulations included the effects of pH and CO_2 concentration, the impacts of mass transport on the local CO_2 concentration and pH and on the observed product distribution could be described as functions of time. While prior studies attempted to simulate the impact of pulsed electrolysis,[3,38,39] none explicitly linked the simulated concentrations to product distributions through an experimentally validated kinetic model.

As shown in **Figure 3b,** the model exhibits good agreement with experimentally observed trends; particularly, the enhancements in C_{2+} FE and total current density upon pulsing. Examination of the simulated transient concentration profiles for CO_2 and pH (**Figure 3d-e**) elucidates the cause for the product enhancements observed during pulsed CO_2R. At the start of the more cathodic portion of the potential pulse, there exists a high transient local concentration of CO_2, consistent with that observed by DEMS, due to replenishment of the local CO_2 concentration during the less cathodic potential hold. Once the potential is made more cathodic, the local pH rises immediately, due to stoichiometric generation of OH^-.[6,40,41] At the same time, the local CO_2 concentration decreases due to increased consumption of CO_2 at more cathodic overpotentials. However, because the rate of decrease in local CO_2 concentration is slower than the rate of increase in local pH, a transient state of high local pH and CO_2 concentration is achieved that facilitates attainment of a C_{2+} FE that is far greater than that attainable by static electrolysis. Pulsing the potential enables repeated access to this metastable state and, hence, improved selectivity.

The continuum model of pulsed electrolysis was used to evaluate the performance of pulsed electrolysis for a broad range of possible potentials, as well as in different bulk electrolytes. This effort showed that a shorter potential pulse (~5 s) could be used to further improve C_{2+} FE by enabling more repeated access to the enhanced transient state. Additionally, the model revealed that pulsed electrolysis substantially favors the generation of CH_4, consistent with experiments when the bicarbonate concentration in the electrolyte was increased because the increased buffer capacity mitigates the increases in pH required to generate C_{2+} products. [42] These results highlight the impact of engineering the microenvironment to enable substantial control on the observed product distributions for CO_2R on Cu.

We note that the effects of pulsed electrolysis on the activity and selectivity of Cu have also been observed on Ag. Work by Azumi has demonstrated that on Ag pulsing increases the FE for CO formation and suppresses that for H_2.[43] The authors attribute the observed enhancement in CO FE to replenishing of the CO_2 at the catalyst surface during the anodic segment of the pulse (*i.e.,* improved CO_2 mass transport).

4.4 Ionomer coated catalysts

As demonstrated for pulsed CO_2 electrolysis, both high local pH and CO_2 concentration are key to increasing the C_{2+} FE during CO_2R on Cu. However, in an aqueous medium, there is an intrinsic tradeoff between these properties due to the parasitic formation of HCO_3^- and $CO_3^=$. This tradeoff can be overcome by coating the Cu catalysts with an ion-conducting polymer (ionomer) that tailors the chemical microenvironment to achieve enhanced CO_2R to C_{2+} products.[44,45] The ionomer composition enables control of ions and water transport through the polymer. **Figure 4** depicts the chemistry and morphology of two standard ionomers: Nafion (a perfluorosulfonic acid, cation-conducting ionomer) and Sustainion (a polystyrene vinylbenzyl methylimidazolium, anion-conducting ionomer).

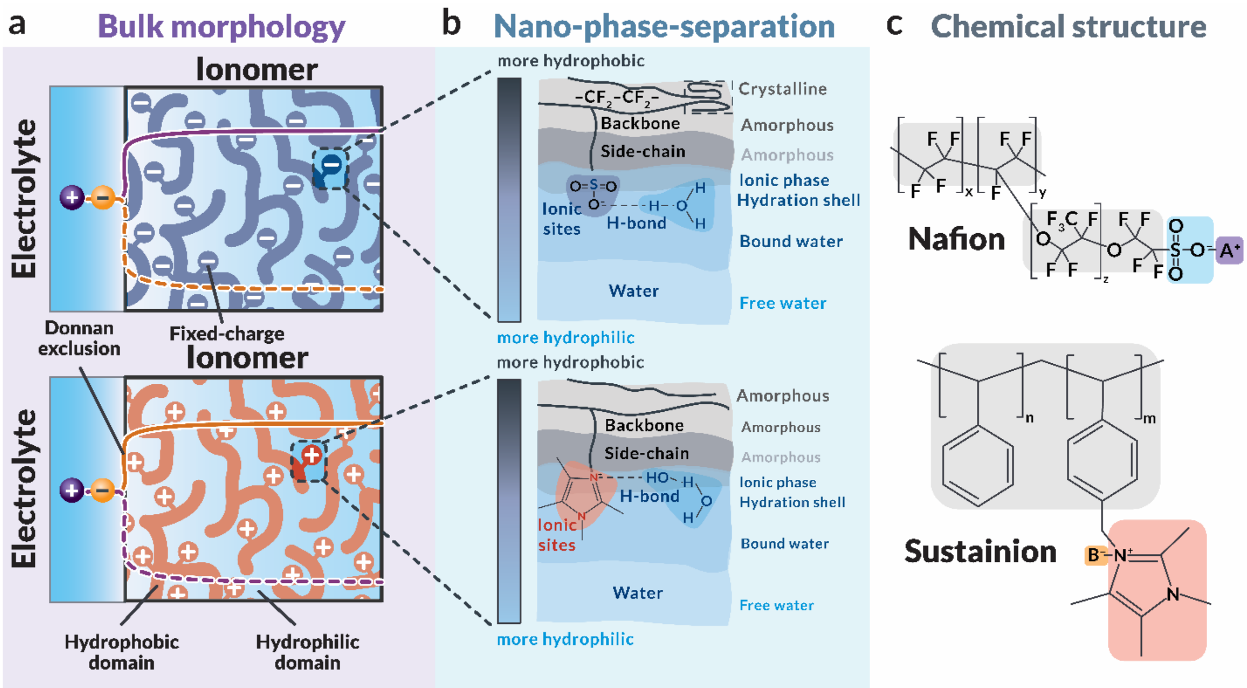

Figure 4: Chemistry and morphology of ionomers. (a) Schematic depiction of the bulk morphology of ionomers. Cation and anion concentration profiles determined by Donnan equilibrium partitioning are shown in the schematic. **(b)** Phase separation at the nanoscale in the ionomers. **(c)** Chemical structure of Nafion and Sustainion ionomers.

Our group has demonstrated that a bi-layer of Nafion and Sustainion facilitates both high local pH and CO_2 concentration, leading to 90% FE to C_{2+} products and only 4% FE to H_2 during pulsed CO_2 electrolysis (**Figure 5**).[4] To understand the role of these ionomer layers, we measured the solubility of water in Nafion (1100 g mol_{eq}^{-1} of equivalent weight) and Sustainion coated on Cu (Naf1100/Cu and Sus/Cu, respectively). The concentration of water decreased in the order bare Cu (aqueous solution) > Sus/Cu > Naf1100/Cu. Sustainion has about 20-fold higher CO_2 solubility than water due to its imidazolium groups, which have a high CO_2 affinity.[46] By contrast, Nafion has a CO_2 solubility comparable to water.[47] Putting these measurements together led to the recognition that the ratio of CO_2/H_2O should increase in the order of bare Cu (aqueous solution) < Naf1100/Cu < Sus/Cu. This order is projected to result in a higher rate of CO_2R compared to HER, which was experimentally confirmed (see **Figure 5**).

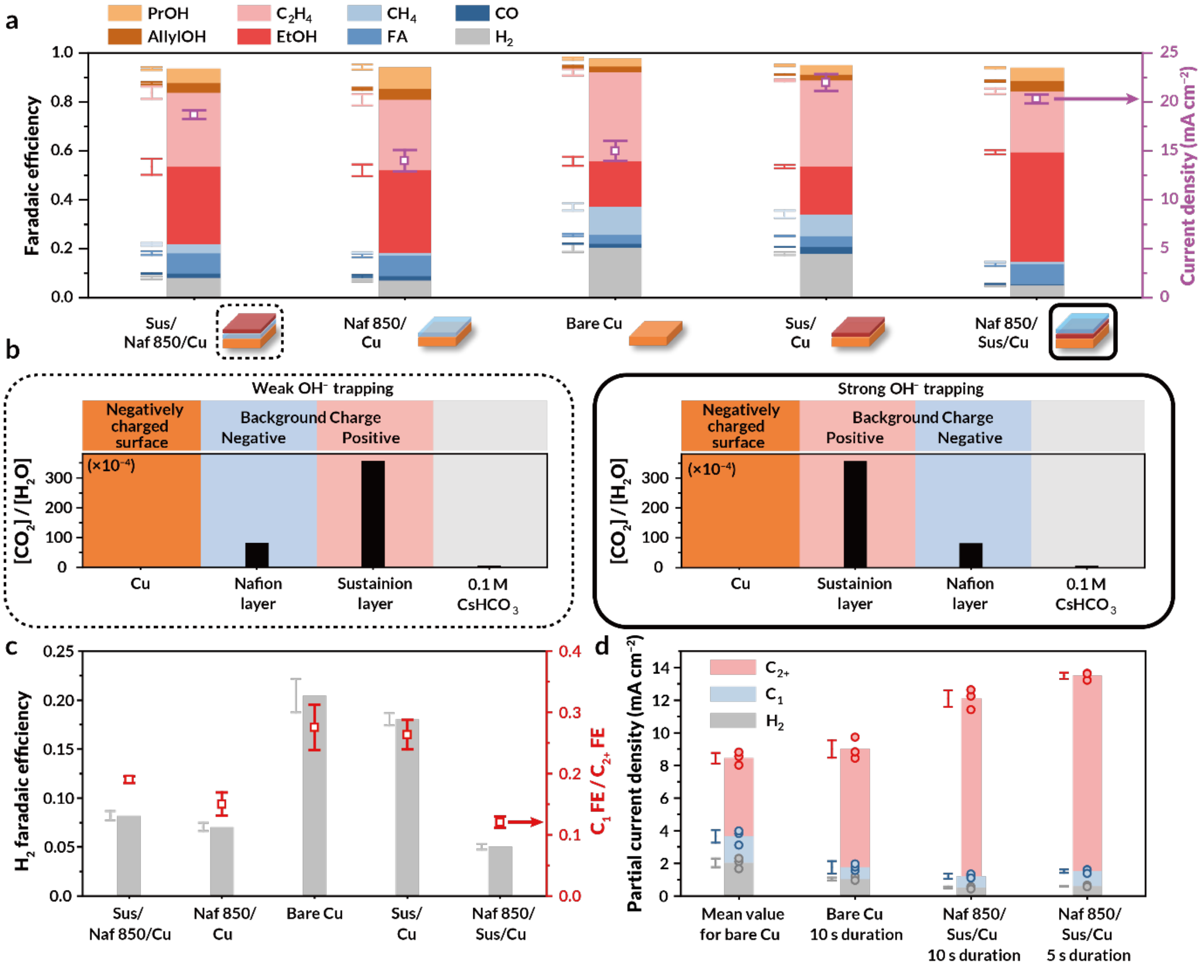

Figure 5: Impact of ionomer layer on CO_2R over Cu catalyst.[4] **(a)** Activity and selectivity obtained for different configurations of the ionomer layers. **(b)** Spatial charge configuration and local $[CO_2]/[H_2O]$ ratio plotted in the various domains of Naf850/Sus/Cu (right) and Sus/Naf850/Cu (left) bilayer ionomer coated catalysts. **(c)** H_2 selectivity and C_1/C_{2+} FE ratio obtained for different configurations of the ionomer layers. **(d)** Partial current densities for different configurations of the ionomer employed in pulsed electrolysis. Adapted with permission from Kim *et al.*[4] Copyright 2021, Springer Science Business Media, LLC.

It is particularly notable that Naf1100/Cu exhibited a higher selectivity to C_{2+} products than bare Cu. Moreover, the C_{2+} selectivity increased further when Naf1100 was replaced with lower equivalent weight Naf850 (850 g mol_{eq}^{-1}), and the i_{CO2R} for Naf850/Cu was lower than that for Naf1100/Cu due to the higher density of hydrophilic sulfonate groups, leading to a lower CO_2/H_2O ratio. Therefore, while the local ratio of CO_2/H_2O explains the enhancement in CO_2R activity, it is not sufficient to describe observed increase in C_{2+} selectivity. Therefore, we postulated that

Donnan exclusion, the thermodynamic exclusion of ions from a polymer matrix of the same sign as that of the background charge (**Figure 4a**),[48] was responsible for the enhanced C_{2+} selectivity due to an accumulation of OH^- generated at the Cu surface and exclusion by the sulfonate groups in Nafion. This explanation was supported experimentally by observation of a significant decrease in the HER current density when Nafion-coated Cu was used for the electrochemical reduction of acetonitrile, a pH-insensitive reaction that suffers from parasitic HER as a side-reaction.[49] Finally, as shown in **Figure 5a-c**, by layering Nafion and Sustainion, an optimal microenvironment for C_{2+} production was found to be Naf/Sus/Cu (Nafion at the outermost layer), which achieved a high local CO_2/H_2O ratio due to the inner Sustainion layer and a high local pH due to OH^- trapping by Nafion. This bi-layer architecture resulted in a 250% improvement in C_{2+} production and a 70% suppression in HER during pulsed CO_2 electrolysis relative to what was observed for bare Cu (see **Figure 5d**).

While our studies of ionomer-coated catalysts have been limited to ionomer-coated Cu, similar studies have recently appeared for Ag. Notably, Lees *et al.* invoke a pH trapping argument, similar to that proposed for Cu, in order to explain why Nafion-coated Ag produces substantial amounts of formic acid, a product typically only observed on Ag only at extremely high pH.[50] And in closely related work, Koshy *et al.* have noted that imidazolium- based ionomer coatings have no effect on CO_2R activity but are able to modulate the activity for HER on Ag.[51] These studies suggest that while some of the ionomer effects we have observed are transferable to Ag, the details of these effects may be chemistry dependent. Hence, further work is needed to explore how ionomers can be used to affect the microenvironment of electrocatalysts used for CO_2R.

5. Porous-electrode systems

A key challenge in the development of CO_2R devices is overcoming mass-transport limitations resulting from the low solubility and diffusivity of CO_2 in aqueous electrolytes.[1,18,52] Planar electrodes used in conjugation with an aqueous electrolyte are useful for characterizing and/or discovering new catalysts and materials. However, they have relatively thick mass-transfer boundary layers (50-200 μm), which impose mass-transport limitations, limiting CO_2R current density to < 100 mA cm^{-2} (**Figure 6a-b**). If CO_2R is to be employed industrially, current densities of > 100 mA cm^{-2} must be achieved.[5] For such applications, devices employing porous electrodes will be necessary (**Figure 6d**). The catalyst layer in a porous electrode is made up of nanoparticles that increase substantially the catalytically active surface area relative to that available for planar electrodes. Furthermore, the porous structure of the catalyst layer enables more direct delivery of gaseous CO_2 through thin, overlapping layers of electrolyte (10-100 nm), which drastically enhances CO_2 transport (**Figure 6e**); such systems have been demonstrated to achieve current densities for CO_2R exceeding 1 A cm^{-2}.[53]

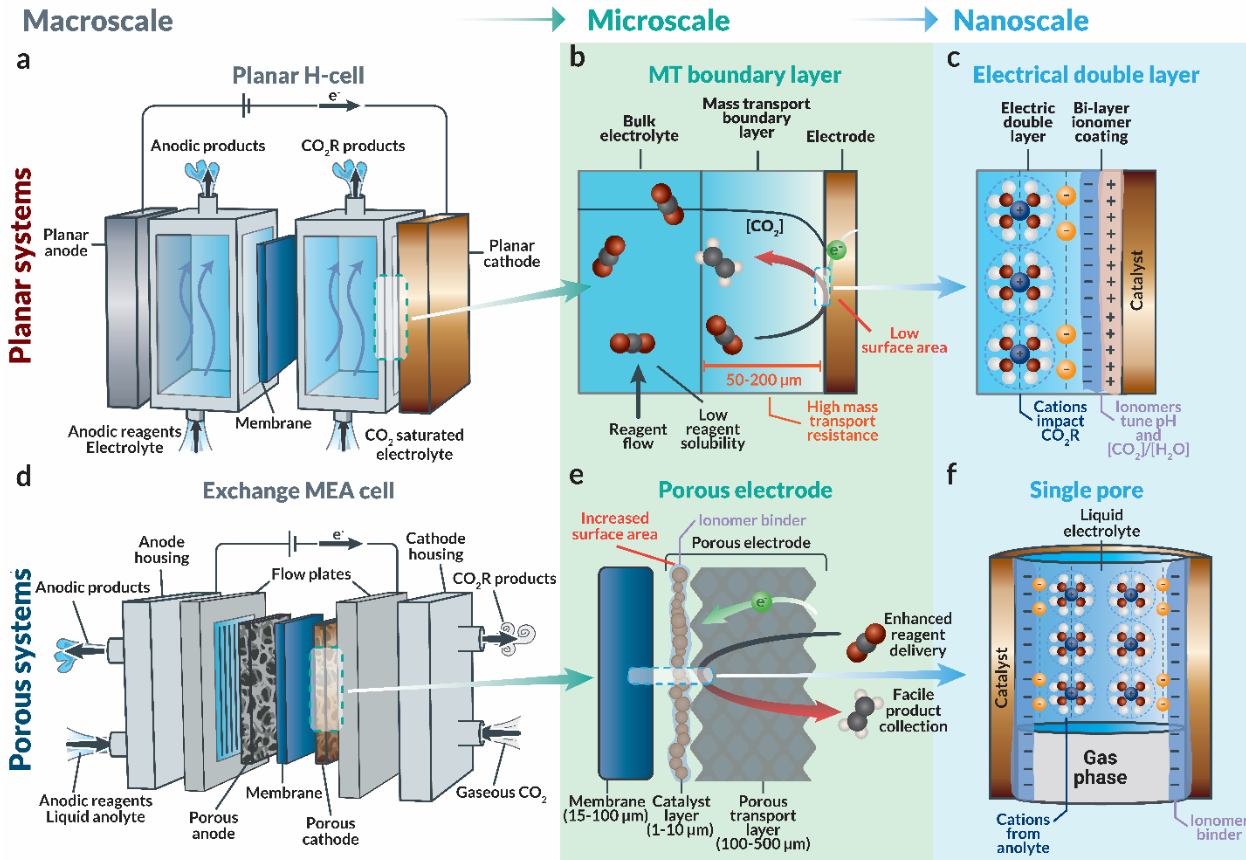

Figure 6: Operation of planar and porous electrode systems at several length scales. (a) Macroscale schematic of a planar H-cell device used for characterizing catalysts for CO_2R. **(b)** Zoomed inset of the mass transport boundary layer in CO_2R on planar Cu. **(c)** Further zoomed inset of the electrical double layer on planar Cu, emphasizing the possibility for cation effects or ionomer layers at the catalyst surface. **(d)** Macroscale schematic of an exchange-MEA device for electrochemical CO_2 reduction. **(e)** Zoomed inset of the porous electrode and the adjacent ion-exchange membrane layer. **(f)** Further zoomed inset of a single pore within the porous electrode.

The most commonly used porous-electrode architecture for CO_2R is the exchange MEA.[50,53–55] In this architecture, gaseous CO_2 is fed into a flow plate that distributes the reactant CO_2. The CO_2 diffuses through a tortuous, porous-transport layer (typically a fibrous carbon layer) that ensures uniform delivery of the CO_2 and electrons to the porous catalyst layer. The catalyst layer, consisting of catalyst nanoparticles dispersed in an ionomer binder, is where the CO_2R occurs. The ionomer binds the particles and provides a pathway for ion conduction. An ion-exchange membrane is employed between the porous electrodes to facilitate ionic conduction between the electrodes, while simultaneously mitigating product crossover. At the anode, an aqueous exchange solution (typically either a hydroxide or a bicarbonate solution) is fed through the porous support for the catalyst layer, wherein water oxidation occurs. The use of an anolyte salt at the anode substantially reduces the ohmic resistance of the overall cell by ensuring the membrane is well hydrated.[40] **Figure 6** illustrates the operation of planar and porous systems over several length scales. Since this Account is devoted to the effects of the catalyst microenvironment on catalyst performance, the issue we focus on is the difference in microenvironments of a catalyst in a porous electrode to that in a planar electrode with an aqueous electrolyte.

There exist multiple critical differences between the microenvironment in an MEA and that for a planar-electrode system. First, the MEA achieves a much higher total current density compared to that for a planar system due to the substantially reduced diffusion length, which increases CO_2 delivery rate.[56] However, the high current densities achieved in an MEA produce substantial electro-osmotic fluxes that pull water from the cathode catalyst layer and substantially reduce its water activity.[6] These fluxes, which do not occur in aqueous systems where the water activity is unity, can drastically skew the ratio of $[CO_2]/[H_2O]$ within the catalyst microenvironment. Lastly, because the diffusion boundary layer in an MEA is quite thin, the effects of pulsed electrolysis, which rely on transient CO_2 and pH changes within the mass-transport boundary layer, may be even greater than those observed for planar electrode systems; hence, future work should evaluate the efficacy of pulsed electrolysis for porous catalyst layers.

We believe that much of the work done by our group on the effects of catalyst microenvironment using planar electrodes is transferable to systems employing porous electrodes. For instance, because it has been shown that cations from the anolyte transport to the cathode catalyst layer during CO_2R in exchange MEAs,[40] the effects of the electrolyte cation are still relevant for porous systems.[54,57] Additionally, the effects of pH and CO_2 availability on the rate of CO_2R are expected to persist in MEAs, as these effects are a result of the intrinsic kinetics of Cu. The selectivity enhancements for ionomer-coated catalysts and pulsed electrolysis were also observed for both metal foils and nanostructured Cu, suggesting that microenvironment effects prevail regardless of the catalyst morphology.[3,4] Therefore, the effects of the ionomer coatings reported here should be transferrable to porous-catalyst layers comprised of nanoparticles surrounded by an ionomer. For porous catalyst layers supported on the surface of a gas-diffusion layer, the transport of CO_2 to the surface of the ionomer layer surrounding the catalyst is rapid, but its transport to the catalyst surface is dictated by the ionomer, as discussed in recent simulation and experimental studies.[58–60] Thus we expect the pH effects incurred by Nafion, and the local increase in CO_2 solubility due to the charged N moieties on Sustainion will likely both remain relevant even in porous catalyst layers. Indeed, prior studies have demonstrated that use of a Nafion binder for a Cu catalyst layer drastically enhances the rate of C_2H_4 generation in a porous electrode, and that increasing the Nafion content improves C_{2+} FE.[53,61] It is important to note, however, that the method of porous-catalyst-layer fabrication typically involves dispersing catalyst particles and ionomer within a solvent and depositing the resulting catalyst-layer ink on the membrane or porous-transport layer. This preparation method poses a significant challenge in the creation of catalyst nanoparticles coated with the kind of distinct bi-layer catalyst coatings developed for the planar system. Thus future work should aim to use techniques such as electrospinning to enable separation of the ionomer binders and facilitate the fabrication of porous catalyst layers with distinct bi-layer ionomer coatings on each nanoparticle.

6. Summary and perspective

This Account demonstrates that not only the composition and surface morphology of the catalyst but also the local microenvironment next to the catalyst surface strongly influence both the catalyst activity and selectivity for the electrochemical reduction of CO_2. We have illustrated how these factors affect both the total current density and the FE for forming C_{2+} products on Cu and CO on Ag. We have shown that a roughened Cu surface enhance exhibits high FE to C_{2+} products and reduced FE to C_1 products and H_2. These effects are largely due to undercoordinated Cu sites on the catalyst surface that bind CO more strongly than do flat facets. Mass-transfer limitations near the catalyst surface, encountered at current densities exceeding about 1 mA/cm^2, result from a rise in the local pH of the electrolyte and a drop in the local concentration of CO_2 due to the combined effects of mass transfer and buffering via the reaction of CO_2 with OH^- anions to form HCO_3^- and CO_3^{2-} anions. Electrolyte cations present near the catalyst surface also enhance the activity and selectivity of Cu and Ag catalysts. The choice of electrolyte cation also has an effect on the activity and selectivity of Cu. Cs^+ cations are present in higher surface concentration in the double layer than cations with a larger radius of hydration, *e.g.,* Li^+. The higher surface-charge density created by hydrated Cs^+ cations produces a proportionately stronger space-charge field, which stabilizes the adsorption of CO_2 and the OC-CO dimer that are precursors to C_{2+} products. Because of these effects, the total current density and the C_{2+} FE are higher in $CsHCO_3$ than $LiHCO_3$. By contrast, the presence of buffering anions, such as HCO_3^- and HPO_4^-, that have low pK_a's relative to H_2O can serve as proton sources that enhance the formation of CH_4 and H_2 at the expense of C_{2+} products. We have also demonstrated that the placement of a thin ionomer film between the surface of Cu and an aqueous electrolyte further alters the microenvironment near the Cu surface. Most notably, covering the surface with an anion-conducting film, such as Sustainion, and then a cation-conducting film, such as Nafion, enables the attainment of a very high C_{2+} FE and concurrently a low H_2 FE. These effects are attributed to creation of a microenvironment in which the ratio of CO_2/H_2O and the pH are significantly higher than that in an aqueous electrolyte. Further enhancement of these properties can be achieved by conducting pulsed electrolysis of CO_2. Finally, we note that the catalyst layer in a membrane-electrode assembly is more complex that that used in a planar-electrode system, opening up additional degrees of freedom for shaping the microenvironment near the catalyst surface.

7. Author biographies

Justin Bui was born in 1997 in Fairfax, VA and received his B. Sc. in Chemical Engineering from Columbia University in 2019. He is currently pursuing his Ph. D. as a NDSEG Fellow at the University of California, Berkeley under the direction of Prof. Alexis Bell and Dr. Adam Weber.

Chanyeon Kim received his B. Sc. and M. Sc. from Yonsei University and his Ph. D. from Korea Advanced Institute of Science and Technology in 2018. He is currently a postdoctoral research fellow under the supervision of Dr. Francesca Toma, Dr. Adam Weber, and Prof. Alexis Bell.

Alex King was born in Cologne, Germany in 1997 and received his B. Sc. in Chemical Engineering at the University of Michigan, Ann Arbor in 2019. He is currently an NSF funded Ph. D. student at the University of California, Berkeley under the advisement of Prof. Alexis Bell and Dr. Adam Weber.

Oyinkansola Romiluyi received her B. Sc. in Chemical Engineering with a minor in Sustainable Energy from the University of Toronto, St. George in 2016. She then received her M. Sc. in Chemical Engineering from Columbia University in 2017. She is currently a Ph. D. Candidate at the University of California, Berkeley and is advised by Prof. Alexis Bell and Dr. Adam Weber.

Ahmet Kusoglu is a Scientist at Berkeley Lab, working on characterization of ionomers and interfaces for electrochemical energy devices and related mechanochemical phenomena. He holds a Ph. D. from University of Delaware, did his post-doctoral research at LBNL, and received the Srinivasan Award of the Electrochemical Society and ECS-Toyota Fellowship.

Adam Weber received a B. Sc. and M. Sc. from Tufts University and his Ph. D. from UC Berkeley in 2004. He is currently a Senior Scientist at LBNL focused on investigating and optimizing electrochemical technologies.

Alexis Bell received his Sc. D. in Chemical Engineering from the Massachusetts Institute of Technology, after which he joined the Department of Chemical and Biomolecular Engineering at the University of California, Berkeley, where he is the Dow Professor of Sustainable Chemistry. His research includes experimental and theoretical studies of heterogeneous catalysis, with a recent emphasis on the electrochemical oxidation of water and the reduction of carbon dioxide.

8. Acknowledgements

This material is based on work performed by the Liquid Sunlight Alliance, which is supported by the U.S. Department of Energy, Office of Science, Office of Basic Energy Sciences, Fuels from Sunlight Hub under Award Number DE-SC0021266. JCB acknowledges funding from the National Science Foundation Graduate Research Fellowship (NSFGRFP) under Grant No. DGE 1752814 and the National Defense Science and Engineering Graduate Fellowship Program. AJK acknowledges funding from the NSFGRFP under Grant No. DGE 1752814. CK acknowledges support from the Basic Science Research Program through the National Research Foundation of Korea (NRF) funded by the Ministry of Education (NRF-2021R1A6A3A14044966).

8. References

(1) Singh, M. R.; Clark, E. L.; Bell, A. T. Effects of Electrolyte, Catalyst, and Membrane Composition and Operating Conditions on the Performance of Solar-Driven Electrochemical Reduction of Carbon Dioxide. *Phys. Chem. Chem. Phys.* **2015**, *17*, 18924–18936. https://doi.org/10.1039/c5cp03283k.

(2) Resasco, J.; Chen, L. D.; Clark, E.; Tsai, C.; Hahn, C.; Jaramillo, T. F.; Chan, K.; Bell, A. T. Promoter Effects of Alkali Metal Cations on the Electrochemical Reduction of Carbon Dioxide. *J. Am. Chem. Soc.* **2017**, *139*, 11277–11287. https://doi.org/10.1021/jacs.7b06765.

(3) Kim, C.; Weng, L. C.; Bell, A. T. Impact of Pulsed Electrochemical Reduction of CO2 on the Formation of C_{2+} Products over Cu. *ACS Catal.* **2020**, *10*, 12403–12413. https://doi.org/10.1021/acscatal.0c02915.

(4) Kim, C.; Bui, J. C.; Luo, X.; Cooper, J. K.; Kusoglu, A.; Weber, A. Z.; Bell, A. T. Tailored Catalyst Microenvironments for CO_2 Electroreduction to Multicarbon Products on Copper Using Bilayer Ionomer Coatings. *Nat. Energy* **2021**, *6*, 1026–1034. https://doi.org/10.1038/s41560-021-00920-8.

(5) Jouny, M.; Luc, W.; Jiao, F. General Techno-Economic Analysis of CO_2 Electrolysis Systems. **2018**. https://doi.org/10.1021/acs.iecr.7b03514.

(6) Weng, L. C.; Bell, A. T.; Weber, A. Z. A Systematic Analysis of Cu-Based Membrane-Electrode Assemblies for CO_2 reduction through Multiphysics Simulation. *Energy Environ. Sci.* **2020**, *13*, 3592–3606. https://doi.org/10.1039/d0ee01604g.

(7) Dinh, C. T.; Burdyny, T.; Kibria, G.; Seifitokaldani, A.; Gabardo, C. M.; Pelayo García De Arquer, F.; Kiani, A.; Edwards, J. P.; De Luna, P.; Bushuyev, O. S.; Zou, C.; Quintero-Bermudez, R.; Pang, Y.; Sinton, D.; Sargent, E. H. CO_2 Electroreduction to Ethylene via Hydroxide-Mediated Copper Catalysis at an Abrupt Interface. *Science (80-.).* **2018**, *360*, 783–787. https://doi.org/10.1126/science.aas9100.

(8) Bui, J. C.; Kim, C.; Weber, A. Z.; Bell, A. T. Dynamic Boundary Layer Simulation of Pulsed CO_2 Electrolysis on a Copper Catalyst. *ACS Energy Lett.* **2021**, *6*, 1181–1188. https://doi.org/10.1021/acsenergylett.1c00364.

(9) Singh, M. R.; Kwon, Y.; Lum, Y.; Ager, J. W.; Bell, A. T. Hydrolysis of Electrolyte Cations Enhances the Electrochemical Reduction of CO_2 over Ag and Cu. *J. Am. Chem. Soc.* **2016**, *138*, 13006–13012. https://doi.org/10.1021/jacs.6b07612.

(10) Singh, M. R.; Goodpaster, J. D.; Weber, A. Z.; Head-Gordon, M.; Bell, A. T. Mechanistic Insights into Electrochemical Reduction of CO_2 over Ag Using Density Functional Theory and Transport Models. *Proc. Natl. Acad. Sci. U. S. A.* **2017**, *114*, E8812–E8821. https://doi.org/10.1073/pnas.1713164114.

(11) Hori, Y.; Kikuchi, K.; Murata, A.; Suzuki, S. Production of Methane and Ethylene in Electrochemical Reduction of Carbon Dioxide At Copper Electrode in Aqueous Hydrogencarbonate Solution. *Chem. Lett.* **1986**, *15*, 897–898. https://doi.org/10.1246/cl.1986.897.

(12) Kuhl, K. P.; Cave, E. R.; Abram, D. N.; Jaramillo, T. F. New Insights into the Electrochemical Reduction of Carbon Dioxide on Metallic Copper Surfaces. *Energy Environ. Sci.* **2012**, *5*, 7050–7059. https://doi.org/10.1039/c2ee21234j.

(13) Hatsukade, T.; Kuhl, K. P.; Cave, E. R.; Abram, D. N.; Jaramillo, T. F. Insights into the Electrocatalytic Reduction of CO_2 on Metallic Silver Surfaces. *Phys. Chem. Chem. Phys.* **2014**, *16*, 13814–13819. https://doi.org/10.1039/c4cp00692e.

(14) Nitopi, S.; Bertheussen, E.; Scott, S. B.; Liu, X.; Engstfeld, A. K.; Horch, S.; Seger, B.; Stephens, I. E. L.; Chan, K.; Hahn, C.; Nørskov, J. K.; Jaramillo, T. F.; Chorkendorff, I. Progress and Perspectives of Electrochemical CO_2 Reduction on Copper in Aqueous Electrolyte. *Chem. Rev.* **2019**, *119*, 7610–7672. https://doi.org/10.1021/acs.chemrev.8b00705.

(15) Gauthier, J. A.; Stenlid, J. H.; Abild-Pedersen, F.; Head-Gordon, M.; Bell, A. T. The Role of Roughening to Enhance Selectivity to C 2+ Products during CO_2 Electroreduction on Copper . *ACS Energy Lett.* **2021**, 3252–3260. https://doi.org/10.1021/acsenergylett.1c01485.

(16) Wang, L.; Nitopi, S. A.; Bertheussen, E.; Orazov, M.; Morales-Guio, C. G.; Liu, X.; Higgins, D. C.; Chan, K.; Nørskov, J. K.; Hahn, C.; Jaramillo, T. F. Electrochemical Carbon Monoxide Reduction on Polycrystalline Copper: Effects of Potential, Pressure, and pH on Selectivity toward Multicarbon and Oxygenated Products. *ACS Catal.* **2018**, *8*, 7445–7454. https://doi.org/10.1021/acscatal.8b01200.

(17) Liu, X.; Schlexer, P.; Xiao, J.; Ji, Y.; Wang, L.; Sandberg, R. B.; Tang, M.; Brown, K. S.; Peng, H.; Ringe, S.; Hahn, C.; Jaramillo, T. F.; Nørskov, J. K.; Chan, K. PH Effects on the Electrochemical Reduction of $CO_{(2)}$ towards C_2 Products on Stepped Copper. *Nat. Commun.* **2019**, *10*, 1–10. https://doi.org/10.1038/s41467-018-07970-9.

(18) Garg, S.; Li, M.; Weber, A. Z.; Ge, L.; Li, L.; Rudolph, V.; Wang, G.; Rufford, T. E. Advances and Challenges in Electrochemical CO_2 Reduction Processes: An Engineering and Design Perspective Looking beyond New Catalyst Materials. *J. Mater. Chem. A* **2020**, *8*, 1511–1544. https://doi.org/10.1039/c9ta13298h.

(19) Casebolt, R.; Levine, K.; Suntivich, J.; Hanrath, T. Pulse Check: Potential Opportunities in Pulsed Electrochemical CO_2 Reduction. *Joule* **2021**, *5*, 1987–2026. https://doi.org/10.1016/j.joule.2021.05.014.

(20) Kibria, M. G.; Edwards, J. P.; Gabardo, C. M.; Dinh, C. T.; Seifitokaldani, A.; Sinton, D.; Sargent, E. H. Electrochemical CO_2 Reduction into Chemical Feedstocks: From Mechanistic Electrocatalysis Models to System Design. *Adv. Mater.* **2019**, *31*. https://doi.org/10.1002/adma.201807166.

(21) Gao, D.; Arán-Ais, R. M.; Jeon, H. S.; Roldan Cuenya, B. Rational Catalyst and Electrolyte Design for CO_2 Electroreduction towards Multicarbon Products. *Nat. Catal.* **2019**, *2*, 198–210. https://doi.org/10.1038/s41929-019-0235-5.

(22) Wuttig, A.; Toste, F. D. The Interface Is a Tunable Dimension in Electricity-driven Organic Synthesis. *Nat. Sci.* **2021**, *1*, 1–13. https://doi.org/10.1002/ntls.20210036.

(23) Zhu, W.; Tackett, B. M.; Chen, J. G.; Jiao, F. Bimetallic Electrocatalysts for CO_2 Reduction. *Top. Curr. Chem.* **2018**, *376*, 1–21. https://doi.org/10.1007/s41061-018-0220-5.

(24) Jhong, H. R. M.; Ma, S.; Kenis, P. J. Electrochemical Conversion of CO_2 to Useful Chemicals: Current Status, Remaining Challenges, and Future Opportunities. *Curr. Opin. Chem. Eng.* **2013**, *2*, 191–199. https://doi.org/10.1016/j.coche.2013.03.005.

(25) Ju, W. E. N.; Bagger, A.; Leonard, N. *Nanostructures for CO_2 Reduction : From Theoretical Insight to Material Design*.

(26) Zhang, Z.; Melo, L.; Jansonius, R. P.; Habibzadeh, F.; Grant, E. R.; Berlinguette, C. P. pH Matters When Reducing CO_2 in an Electrochemical Flow Cell. *ACS Energy Lett.* **2020**, *5*, 3101–3107. https://doi.org/10.1021/acsenergylett.0c01606.

(27) Clark, E. L.; Bell, A. T. Direct Observation of the Local Reaction Environment during the Electrochemical Reduction of CO_2. *J. Am. Chem. Soc.* **2018**, *140*, 7012–7020. https://doi.org/10.1021/jacs.8b04058.

(28) Newman, J.; Thomas-Alyea, K. E. *Electrochemical Systems*, 3rd ed.; John Wiley and Sons, Inc.: Hoboken, NJ, 2004.

(29) Ringe, S.; Clark, E. L.; Resasco, J.; Walton, A.; Seger, B.; Bell, A. T.; Chan, K. Understanding Cation Effects in Electrochemical CO_2 Reduction. *Energy Environ. Sci.* **2019**, *12*, 3001–3014. https://doi.org/10.1039/c9ee01341e.

(30) Resasco, J.; Lum, Y.; Clark, E.; Zeledon, J. Z.; Bell, A. T. Effects of Anion Identity and Concentration on Electrochemical Reduction of CO_2. *ChemElectroChem* **2018**, *5*, 1064–1072. https://doi.org/10.1002/celc.201701316.

(31) Arán-Ais, R. M.; Scholten, F.; Kunze, S.; Rizo, R.; Roldan Cuenya, B. The Role of in Situ Generated Morphological Motifs and Cu(i) Species in C2+ Product Selectivity during CO_2 Pulsed Electroreduction. *Nat. Energy* **2020**, *5*, 317–325. https://doi.org/10.1038/s41560-020-0594-9.

(32) Hori, Y.; Konishi, H.; Futamura, T.; Murata, A.; Koga, O.; Sakurai, H.; Oguma, K. "deactivation of Copper Electrode" in Electrochemical Reduction of CO_2. *Electrochim. Acta* **2005**, *50*, 5354–5369. https://doi.org/10.1016/j.electacta.2005.03.015.

(33) Shiratsuchi, R.; Aikoh, Y.; Nogami, G. Pulsed Electroreduction of CO_2 on Copper Electrodes. *J. Electrochem. Soc.* **1993**, *140*, 3479–3482. https://doi.org/10.1149/1.2221113.

(34) Yano, J.; Yamasaki, S. Pulse-Mode Electrochemical Reduction of Carbon Dioxide Using Copper and Copper Oxide Electrodes for Selective Ethylene Formation. *J. Appl. Electrochem.* **2008**, *38*, 1721–1726. https://doi.org/10.1007/s10800-008-9622-3.

(35) Kumar, B.; Brian, J. P.; Atla, V.; Kumari, S.; Bertram, K. A.; White, R. T.; Spurgeon, J. M. Controlling the Product Syngas H_2:CO Ratio through Pulsed-Bias Electrochemical Reduction of CO_2 on Copper. *ACS Catal.* **2016**, *6*, 4739–4745. https://doi.org/10.1021/acscatal.6b00857.

(36) Engelbrecht, A.; Uhlig, C.; Stark, O.; Hämmerle, M.; Schmid, G.; Magori, E.; Wiesner-Fleischer, K.; Fleischer, M.; Moos, R. On the Electrochemical CO_2 Reduction at Copper

Sheet Electrodes with Enhanced Long-Term Stability by Pulsed Electrolysis . *J. Electrochem. Soc.* **2018**, *165*, J3059–J3068. https://doi.org/10.1149/2.0091815jes.

(37) Kimura, K. W.; Fritz, K. E.; Kim, J.; Suntivich, J.; Abruña, H. D.; Hanrath, T. Controlled Selectivity of CO_2 Reduction on Copper by Pulsing the Electrochemical Potential. *ChemSusChem* **2018**, *11*, 1781–1786. https://doi.org/10.1002/cssc.201800318.

(38) Kimura, K. W.; Casebolt, R.; Cimada Dasilva, J.; Kauffman, E.; Kim, J.; Dunbar, T. A.; Pollock, C. J.; Suntivich, J.; Hanrath, T. Selective Electrochemical CO_2 Reduction during Pulsed Potential Stems from Dynamic Interface. *ACS Catal.* **2020**, *10*, 8632–8639. https://doi.org/10.1021/acscatal.0c02630.

(39) Gupta, N.; Gattrell, M.; MacDougall, B. Calculation for the Cathode Surface Concentrations in the Electrochemical Reduction of CO_2 in $KHCO_3$ Solutions. *J. Appl. Electrochem.* **2006**, *36*, 161–172. https://doi.org/10.1007/s10800-005-9058-y.

(40) Weng, L. C.; Bell, A. T.; Weber, A. Z. Towards Membrane-Electrode Assembly Systems for CO_2 Reduction: A Modeling Study. *Energy Environ. Sci.* **2019**, *12*, 1950–1968. https://doi.org/10.1039/c9ee00909d.

(41) Yang, K.; Kas, R.; Smith, W. A. In Situ Infrared Spectroscopy Reveals Persistent Alkalinity near Electrode Surfaces during CO_2 Electroreduction. *J. Am. Chem. Soc.* **2019**, *141*. https://doi.org/10.1021/jacs.9b07000.

(42) Casebolt, R.; Kimura, K. W.; Levine, K.; Cimada DaSilva, J. A.; Kim, J.; Dunbar, T. A.; Suntivich, J.; Hanrath, T. Effect of Electrolyte Composition and Concentration on Pulsed Potential Electrochemical CO_2 Reduction. *ChemElectroChem* **2020**, 681–688. https://doi.org/10.1002/celc.202001445.

(43) Oguma, T.; Azumi, K. Improvement of Electrochemical Reduction of CO_2 using the Potential-Pulse Polarization Method. *Electrochemistry* **2020**, *88*, 451–456. https://doi.org/10.5796/electrochemistry.20-00037.

(44) Crothers, A. R.; Darling, R. M.; Kusoglu, A.; Radke, C. J.; Weber, A. Z. Theory of Multicomponent Phenomena in Cation-Exchange Membranes: Part I. Thermodynamic Model and Validation. *J. Electrochem. Soc.* **2020**, *167*, 013547. https://doi.org/10.1149/1945-7111/ab6723.

(45) Aeshala, L. M.; Uppaluri, R.; Verma, A. Electrochemical Conversion of CO_2 to Fuels: Tuning of the Reaction Zone Using Suitable Functional Groups in a Solid Polymer Electrolyte. *Phys. Chem. Chem. Phys.* **2014**, *16*, 17588–17594. https://doi.org/10.1039/c4cp02389g.

(46) Sadeghpour, M.; Yusoff, R.; Aroua, M. K. Polymeric Ionic Liquids (PILs) for CO_2 Capture. *Rev. Chem. Eng.* **2017**, *33*, 183–200. https://doi.org/10.1515/revce-2015-0070.

(47) Ren, X.; Myles, T. D.; Grew, K. N.; Chiu, W. K. S. Carbon Dioxide Transport in Nafion 1100 EW Membrane and in a Direct Methanol Fuel Cell. *J. Electrochem. Soc.* **2015**, *162*, F1221–F1230. https://doi.org/10.1149/2.0711510jes.

(48) Kamcev, J.; Galizia, M.; Benedetti, F. M.; Jang, E. S.; Paul, D. R.; Freeman, B. D.; Manning, G. S. Partitioning of Mobile Ions between Ion Exchange Polymers and Aqueous

Salt Solutions: Importance of Counter-Ion Condensation. *Phys. Chem. Chem. Phys.* **2016**, *18*, 6021–6031. https://doi.org/10.1039/c5cp06747b.

(49) Xia, R.; Tian, D.; Kattel, S.; Hasa, B.; Shin, H.; Ma, X.; Chen, J. G.; Jiao, F. Electrochemical Reduction of Acetonitrile to Ethylamine. *Nat. Commun.* **2021**, *12*, 1–8. https://doi.org/10.1038/s41467-021-22291-0.

(50) Lees, E. W.; Mowbray, B. A. W.; Salvatore, D. A.; Simpson, G. L.; Dvorak, D. J.; Ren, S.; Chau, J.; Milton, K. L.; Berlinguette, C. P. Linking Gas Diffusion Electrode Composition to CO_2 reduction in a Flow Cell. *J. Mater. Chem. A* **2020**, *8*, 19493–19501. https://doi.org/10.1039/d0ta03570j.

(51) Koshy, D. M.; Akhade, S. A.; Shugar, A.; Abiose, K.; Shi, J.; Liang, S.; Oakdale, J. S.; Weitzner, S. E.; Varley, J. B.; Duoss, E. B.; Baker, S. E.; Hahn, C.; Bao, Z.; Jaramillo, T. F. Chemical Modifications of Ag Catalyst Surfaces with Imidazolium Ionomers Modulate H_2 Evolution Rates during Electrochemical CO_2 Reduction. *J. Am. Chem. Soc.* **2021**, *143*, 14712–14725. https://doi.org/10.1021/jacs.1c06212.

(52) Higgins, D.; Hahn, C.; Xiang, C.; Jaramillo, T. F.; Weber, A. Z. Gas-Diffusion Electrodes for Carbon Dioxide Reduction: A New Paradigm. *ACS Energy Lett.* **2019**, *4*, 317–324. https://doi.org/10.1021/acsenergylett.8b02035.

(53) García de Arquer, F. P.; Dinh, C. T.; Ozden, A.; Wicks, J.; McCallum, C.; Kirmani, A. R.; Nam, D. H.; Gabardo, C.; Seifitokaldani, A.; Wang, X.; Li, Y. C.; Li, F.; Edwards, J.; Richter, L. J.; Thorpe, S. J.; Sinton, D.; Sargent, E. H. CO_2 Electrolysis to Multicarbon Products at Activities Greater than 1 A Cm−2. *Science (80-.).* **2020**, *367*, 661–666. https://doi.org/10.1126/science.aay4217.

(54) Huang, J. E.; Li, F.; Ozden, A.; Rasouli, A. S.; de Arquer, F. P. G.; Liu, S.; Zhang, S.; Luo, M.; Wang, X.; Lum, Y.; Xu, Y.; Bertens, K.; Miao, R. K.; Dinh, C. T.; Sinton, D.; Sargent, E. H. CO_2 Electrolysis to Multicarbon Products in Strong Acid. *Science (80-.).* **2021**, *372*, 1074–1078. https://doi.org/10.1126/science.abg6582.

(55) Gabardo, C. M.; O'Brien, C. P.; Edwards, J. P.; McCallum, C.; Xu, Y.; Dinh, C. T.; Li, J.; Sargent, E. H.; Sinton, D. Continuous Carbon Dioxide Electroreduction to Concentrated Multi-Carbon Products Using a Membrane Electrode Assembly. *Joule* **2019**, *3*, 2777–2791. https://doi.org/10.1016/j.joule.2019.07.021.

(56) Weng, L. C.; Bell, A. T.; Weber, A. Z. Modeling Gas-Diffusion Electrodes for CO_2 Reduction. *Phys. Chem. Chem. Phys.* **2018**, *20*, 16973–16984. https://doi.org/10.1039/c8cp01319e.

(57) Fink, A. G.; Lees, E. W.; Zhang, Z.; Ren, S.; Delima, R. S.; Berlinguette, C. P. Impact of Alkali Cation Identity on the Conversion of HCO_3^- to CO in Bicarbonate Electrolyzers. *ChemElectroChem* **2021**, *8*, 2094–2100. https://doi.org/10.1002/celc.202100408.

(58) Nesbitt, N. T.; Burdyny, T.; Simonson, H.; Salvatore, D.; Bohra, D.; Kas, R.; Smith, W. A. Liquid-Solid Boundaries Dominate Activity of CO_2 Reduction on Gas-Diffusion Electrodes. *ACS Catal.* **2020**, *10*, 14093–14106. https://doi.org/10.1021/acscatal.0c03319.

(59) Moore, T.; Xia, X.; Baker, S. E.; Duoss, E. B.; Beck, V. A. Elucidating Mass Transport

Regimes in Gas Diffusion Electrodes for CO_2 Electroreduction. *ACS Energy Lett.* **2021**, *6*, 3600–3606. https://doi.org/10.1021/acsenergylett.1c01513.

(60) Weng, L. C.; Bell, A. T.; Weber, A. Z. Modeling Gas-Diffusion Electrodes for CO_2 reduction. *Phys. Chem. Chem. Phys.* **2018**, *20*, 16973–16984. https://doi.org/10.1039/c8cp01319e.

(61) Guzmán, H.; Zammillo, F.; Roldán, D.; Galletti, C.; Russo, N.; Hernández, S. Investigation of Gas Diffusion Electrode Systems for the Electrochemical CO_2 Conversion. *Catalysts*. 2021. https://doi.org/10.3390/catal11040482.